Emergence of extreme events in a quasiperiodic oscillator

Premraj Durairaj [,1] Sathiyadevi Kanagaraj [,1] Suresh Kumarasamy [,1] and Karthikeyan Rajagopal[1,2]

[1]*Centre for Nonlinear Systems, Chennai Institute of Technology, Chennai 600 069, Tamilnadu, India*
[2]*Department of Electronics and Communications Engineering, University Centre for Research and Development,*
Chandigarh University, Mohali 140 413, Punjab, India

Extreme events are unusual and rare large-amplitude fluctuations can occur unexpectedly in nonlinear dynamical systems. Events above the extreme event threshold of the probability distribution of a nonlinear process characterize extreme events. Different mechanisms for the generation of extreme events and their prediction measures have been reported in the literature. Based on the properties of extreme events, such as those that are rare in the frequency of occurrence and extreme in amplitude, various studies have shown that extreme events are both linear and nonlinear in nature. Interestingly, in this Letter, we report on a special class of extreme events which are nonchaotic and nonperiodic. These nonchaotic extreme events appear in between the quasiperiodic and chaotic dynamics of the system. We report the existence of such extreme events with various statistical measures and characterization techniques.

Extreme events are unanticipated, rare events that occur in many natural and engineering systems. Extreme events (EEs) can exist in various forms, including floods, cyclones, droughts, pandemics, power outages, material ruptures, explosions, chemical contamination, and stock market crashes, among others [1]. Such events have a severe impact on real-world situations. Thus, it is necessary to understand the relevant mechanism and its generic characteristics for the occurrence of EEs in order to prevent such EEs. As a result, researchers have focused on exploring EEs in diverse nonlinear oscillators [2–5], maps [6], and neural networks [7]. Further, extreme events have also been identified in a superfluid helium [8], plasma [9], optical fibers [10], lasers [11], and capillary waves [12], etc.

However, depending on the characteristics of a dynamical system, the occurrence of EEs has been discovered under a variety of mechanisms, including internal crises, on-off intermittency, blowout bifurcations, stick-slip bifurcations, and so on [6,11,13–15]. For instance, prior studies reveal that EEs can arise as a result of the abrupt expansion and destruction of chaotic attractors produced by internal or external crises [11,14]. Further, interior crises are found to be a critical mechanism for the occurrence of EEs, when the trajectory of chaotic attractors reaches the stable manifold of a saddle or unstable periodic orbit, which increases the size of the chaotic attractors. Such a sudden expansion of the chaotic attractor may result in an EE. In addition, Pomeau-Manneville intermittency is identified as another mechanism for the existence of EEs. Such intermittency can occur when periodic oscillations are interspersed by chaotic bursts, which further results in very large-amplitude events. EEs can also exist through the following other mechanisms. The sliding bifurcation near the discontinuous boundary can cause an EE. The trajectory of the attractors might hop between coexisting attractors due to

noise in multistable systems, which can cause unusually large events. This is referred to as noise-induced intermittency. The trajectory of the attractors in coupled systems departs from the synchronization manifold to the transverse direction of the manifold. During such a transition, a synchronization error of dynamics can show to be zero or nonzero and is referred to as on-off intermittency [16].

Moreover, previous studies discovered that extreme or rare events can occur as a result of chaotic or stochastic processes [16]. In particular, the appearance of EEs has been reported in microelectromechanical cantilevers with discontinuous boundaries and diode lasers with phase-conjugate feedback [17,18]. By applying harmonic pump modulation to a fiber laser, the emergence of rogue waves has been identified [2,19–21]. The EEs in stochastic transport on networks has been demonstrated using multiple random walks on complex networks [22,23]. Now, the interesting question is whether extreme events can be induced by nonchaotic signals. In the literature, a study has shown nonchaotic and nonperiodic signals have been well studied in the name of strange nonchaotic dynamics, which arises during the attractor transition from quasiperiodicity to chaos [24]. One can find the generation mechanisms of these strange nonchaotic attractors in the literature [24–26]. The results in the present Letter show that similar to the strange nonchaotic dynamics, the nonperiodic and nonchaotic dynamics show large-amplitude extreme events. The present Letter opens a different area of study where the nonchaotic nonlinear process can also lead to extreme events.

To show the nonchaotic extreme events, we consider a Morse oscillator (MO) which is used to describe the motion of diatomic molecules. Importantly, the MO has made substantial contributions in the fields of classical, semiclassical, and quantum mechanics [27,28]. The MO was used for
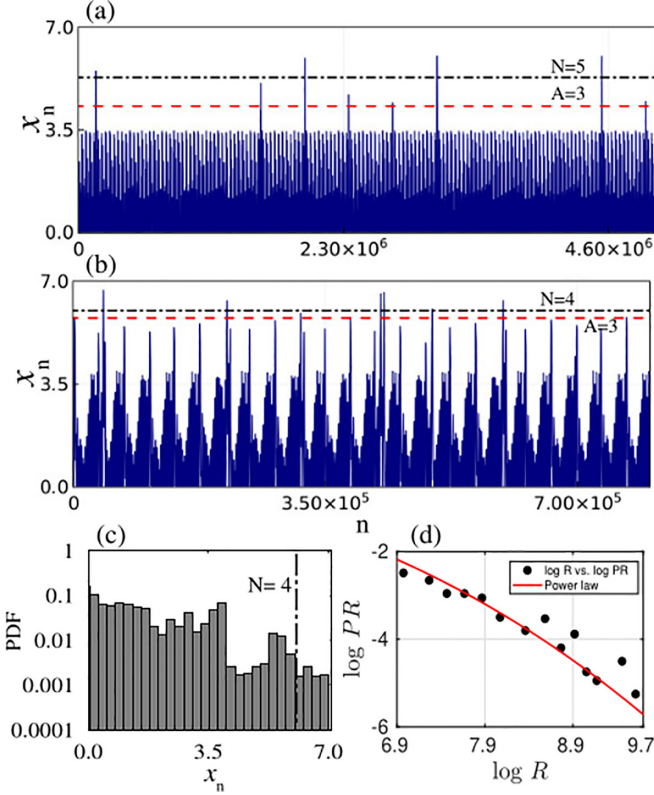
FIG. 1. (a) Time evolution of x_n for the nonchaotic dynamics with forcing amplitudes as (a) $f = g = 0.255$, and (b) $f = g = 0.278$. The x_n is the nth local peaks of the variable x. The horizontal black dotted-dashed and red dashed lines are the critical threshold lines defining the extreme events (refer to the text for the meaning of N and A). (c) The probability distribution function corresponds to the extreme events and (d) return interval (R) (interevent interval) with respect to the probability of recurrence times (PR) of the EE for (b). The solid circles and solid lines in (d) represent the numerical data and the corresponding power-law fit. We fixed the other parameter values as $\gamma = 0.35$, $\omega_1 = 0.3$, and $\omega_2 = (\frac{\sqrt{5}-1}{2})$.

photodissociation molecules without any damping. In the presence of driving and damping, the MO was exploited for multiphoton excitation of molecules, pumping the local mode of polyatomic molecules [29]. We consider a quasiperiodically forced MO and its dynamical equation can be written as

$$\dot{x} = y,$$
$$\dot{y} = f \sin(\omega_1 t) + g \sin(\omega_2 t) + e^{-2x} - e^{-x} - \gamma y, \quad (1)$$

where x and y are the state variables of the system and γ is a damping parameter. The amplitudes of the first and second force are represented by f and g and the corresponding frequencies are denoted by ω_1 and ω_2, respectively.

To manifest the existence of extreme events, we first depicted the time evolution of the x variable in Figs. 1(a) and 1(b) by fixing the amplitude of the first and second forcing as $f = g = 0.255$ and $f = g = 0.278$. We observe from Fig. 1(a) that some of the oscillation (event) has larger amplitudes, while the rest of them take lower amplitudes. To check whether the larger-amplitude oscillations satisfy the extreme

event criteria defined in the literature, we use the following relation,

$$x_{\mathrm{EE}} = \langle x_n \rangle + N\sigma_{x_n}, \quad (2)$$

where x_{EE} is the critical amplitude threshold and N is a multiplication factor. The mean and standard deviation of the variable x is represented by $\langle x_n \rangle$ and σ_{x_n}, respectively. Here, the x_n (an event) are the local peaks of the variable x. An event or a local peak can satisfy extreme event criteria if it has a value higher than the critical threshold defined by Eq. (2) with $N \geqslant 4$. To confirm the presence of EE, we plotted the critical threshold on the time series for $N = 5$ and $N = 4$ in Figs. 1(a) and 1(b). We used two different N values depending on the time series. Though the choice of N is arbitrary, we set the minimum N value as 4 in the present study. We also find the critical value of $N_{\max}$ for a range of each f value—the details will be discussed below. In both cases, we can see that some of the large-amplitude events cross the threshold line, confirming the presence of EE. Since the choice of N is arbitrary in the previous criterion, we use another criterion defined by the abnormality index, $A_n = \frac{Hf_n}{H_{1/3}}$ [17], where Hf_n is the difference between the maximum height of the event n and the mean height of its population, $Hf_n = x_n - \langle x_n \rangle_n$, and $H_{1/3}$ is the average value among the highest one-third values of Hf_n. If an event x_n has abnormality A_n greater than 2, then the event is termed an extreme event. We find that both cases in Figs. 1(a) and 1(b) satisfy the above criterion with abnormality index $A = 3$ denoted by a dashed horizontal line in the plots. It is evident that a few rare large-amplitude events cross the abnormality index line. We computed the probability distribution function (PDF) in Fig. 1(c) for the time series shown in Fig. 1(b). The EE critical threshold at $N = 4$ is plotted as a vertical dashed line on the PDF diagram. In the plot, the events with a finite probability above the critical threshold line characterize the extreme events. We can plot a similar probability distribution for Fig. 1(a), however, for simplicity, we have plotted the PDF corresponding to Fig. 1(b).

The above analysis shows that the observed behavior satisfies the extreme event criterion in the amplitudes. Another important characteristic of extreme events is an interevent interval. The interevent interval defines the frequency occurrence of the events and should not have discrete values (discrete values mean the periodic occurrence of events), rather it should have a distribution over a range. In order to examine the distribution of events in the observed time series, we find interevent intervals (R) between successive extreme events. Subsequently, we find the probability of such interevent intervals (PR) as shown in Fig. 1(d). The interevent interval and its probability obey power-law relations as given by $\log_{10}(\mathrm{PR}) = a\log_{10}(\mathrm{R})^b$, where a and b are constants with values $a = -0.006$ and $b = 2.96$, respectively. The obtained numerical values are depicted in a solid circle, and a continuous line shows the corresponding power-law fit. The route for the emergence of EE and its transitions is further estimated below using Lyapunov exponents (LEs), amplitude maxima $X_{\max}$, critical factor $N_{\max}$, and a two-parameter analysis.

To illustrate the global dynamical transition of the attractors and route of the EE, the two-parameter diagram is drawn in (f, g) space using the maximum LE as shown
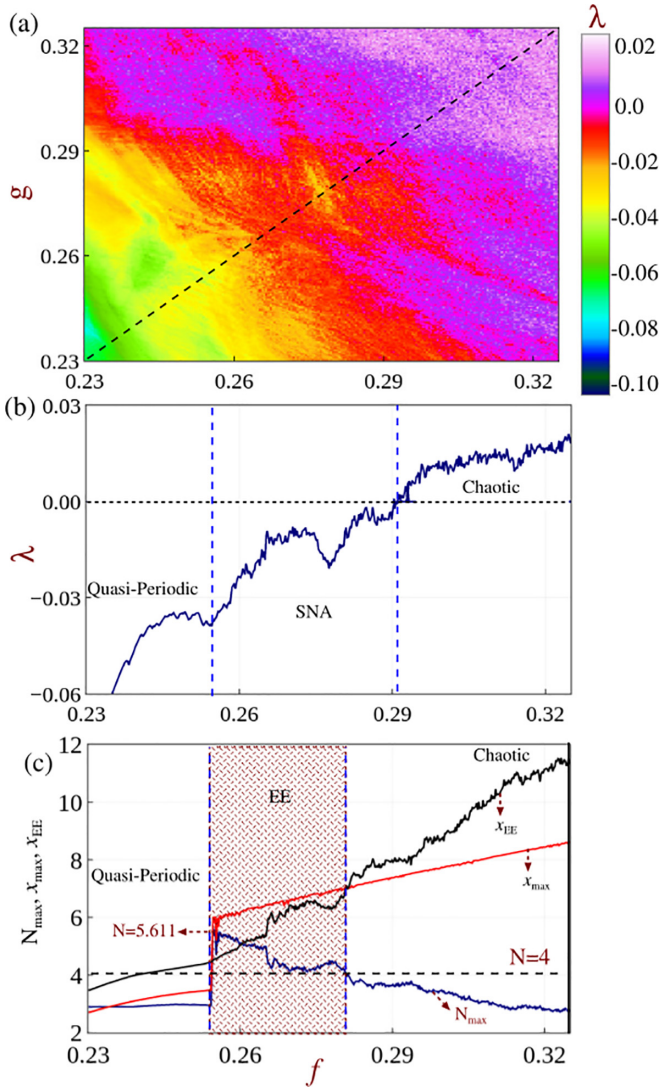
FIG. 2. (a) The two-parameter bifurcation diagram in (f, g) space. Using the range of Lyapunov exponents (λ) (denoted by the color bar) the dynamical regions are marked. (b) The maximum Lyapunov exponents as a function of forcing amplitude $f(= g)$, (c) Maximum amplitude of the events x_{max} (red) and the corresponding N_{max} [Eq. (3)] of the event (blue) by varying the magnitude of $f(= g)$. The black line represents the extreme event critical threshold (x_{EE}) drawn from Eq. (2) for $N = 4$. The other parameter values are fixed as in Fig. 1.

in Fig. 2(a). The range of LE (shown in the color bar) denotes the emergence of quasiperiodic, nonchaotic, and chaotic attractors in the respective parameters of f and g. If the forcing amplitudes f and g are small, attractors have a maximum negative LE, indicating the presence of a quasiperiodic (QP) attractor region. To better comprehend QP attractors, we plotted their time-evolution and phase portrait trajectories in the Supplemental Material Figs. S1(a)(i) and S1(a)(ii) [30] for $f = g = 0.23$, which show their bounded nature. Thus, the EE critical threshold for this attractor is greater than the amplitude of QP attractors. By increasing f and g values, the QP attractor transits to a chaotic (CH) attractor via strange and nonchaotic dynamics in which the LE takes the

values from negative (near zero) to positive. To distinguish between the strange nonchaotic and chaotic attractors, the time-evolution and phase portrait trajectories are shown in Figs. S1(b)(i) and S1(b)(ii) and Figs. S1(c)(i) and S1(c)(ii) in the Supplemental Material [30] by fixing $f = g = 0.278$ and $f = g = 0.33$, respectively. Also, the frequency spectra can be used to distinguish quasiperiodic, strange nonchaotic attractor (SNA), and chaos. We have the frequency spectrum analysis in the Supplemental Material in Figs. S4(a)– S4(c) [30]. When compared to the chaotic attractor (which has a greater number of large-amplitude oscillations), we found the SNA shows fewer large-amplitude oscillations. The Supplemental Material's Fig. S1 [30] can be consulted for more information. Furthermore, to show the dynamical transitions clearly, we displayed maximum Lyapunov exponents in Fig. 2(b) by keeping the parameter $(f = g)$ and varying it along the diagonal dashed line shown in Fig. 2(a). In Fig. 2(b), the maximum LE is illustrated as a function of forcing amplitudes f and g ($f = g$) in the range $[0.23 < f(= g) < 0.32]$. We observe that when the forcing amplitudes are minimum in the mentioned range, LE takes negative values, indicating quasiperiodic dynamics. While increasing the parameter, the transition of LE from negative to positive values indicates the dynamical transition of quasiperiodic behavior to chaotic behavior. Furthermore, we found that the negative values of LE near zero exhibit strange nonchaotic behavior; extreme events are seen in this region. The literature has shown that the EEs occur under chaotic dynamics [16] through distinct routes, and stochastic processes such as stochastic transport on networks have been demonstrated using multiple random walks on complex networks [22,23]. Among the various routes, the occurrence of EEs in nonchaotic dynamics is different.

To validate the occurrence of EEs in the SNA region, we find the maximum amplitude x_{max}, extreme event threshold x_{EE}, and maximum value of N (N_{max}) of a given time series. In Fig. 2(c), we have plotted the above quantities by varying the magnitude of $f = g$. The plot explains the regime of extreme events in the following way. During the nonextreme regime, the critical threshold x_{EE} is larger than the x_{max}. It means that the threshold is larger than the large-amplitude oscillations and does not satisfy the extreme event criterion. While in the EE regime, the x_{max} is larger than the EE critical threshold x_{EE} (shaded EE region). This explains that extreme events have a larger amplitude than the extreme event criterion. Note that the SNA regime in the parameter range $f \in 0.28$–0.2912 shows no extreme events. As we discussed above, we fixed $N = 4$ as an arbitrary constant from the literature [31]. However, the maximum value of the N can be determined by rewriting Eq. (2) as

$$N_{max} = \frac{\max(x_{EE}) - \langle x_n \rangle}{\sigma_{x_n}}. \qquad (3)$$

In the SNA region shown in Fig. 2(c), we found that the multiplication factor taking values between $4 \leqslant N_{max} \leqslant 5.611$ when the forcing amplitudes are in the range from 0.256 to 0.28 denoted by the shaded transparent pattern. The plot of N_{max} shows that depending on the parameter choice, the arbitrary value can be chosen $N \in \{4, 5.611\}$. Thus the above results satisfy all the criteria proposed for the extreme events and justify the existence of EEs in the SNA regime.
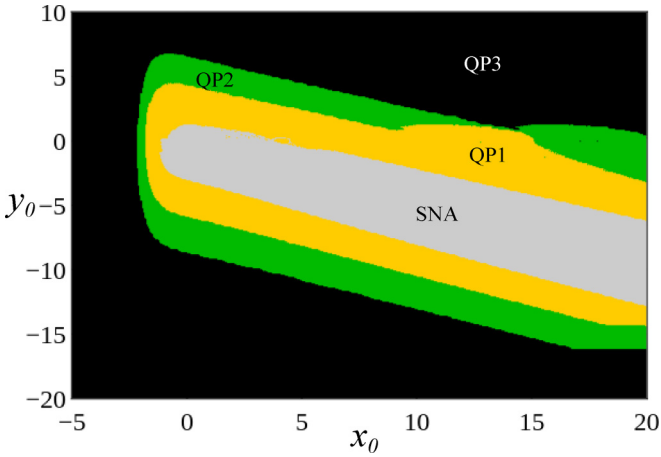
FIG. 3. Basin of attraction for $f = g = 0.278$. QP1, QP2, and QP3 are the quasiperiodic attractor 1, quasiperiodic attractor 2, and quasiperiodic attractor 3, respectively. SNA represents the strange nonchaotic attractor. We fixed the other parameter values the same as in Fig. 1.

FIG. 4. Two-parameter phase diagram in (f, g) space [plotted using Eq. (2) for fixed initial condition $(x_0, y_0) = (0.3, 0.2)$], to distinguish the existence of extreme events (EE) and nonextreme events (NEE), respectively. We fixed the other parameter values as in Fig. 1.

As we discussed earlier, the observed EEs are nonchaotic and nonperiodic. At the same time, the parameters corresponding to the strange nonchaotic EEs show multiple stable behaviors. The multistable behavior can be seen from the basins of attraction drawn for a range of initial conditions. Figure 3 is drawn by varying the initial states x_0 and y_0 of the system for the parameters given in the caption to Fig. 1. We can see that the basin of nonchaotic and nonperiodic behavior or SNA is embedded within the basin of quasiperiodic dynamics. Outside the SNA basin, we have found three different basins which contain quasiperiodic attractors. All the three different quasiperiodic attractor basins and the SNA basin, denoted by QP1, QP2, QP3, and SNA, respectively, are shown in Fig. 3. In Supplemental Material Fig. S2 [30], each of the quasiperiodic attractors is depicted. Figure 3 shows that extreme events occur for specific values of initial conditions. The size of these basins changes as we vary the parameter within the EE regime marked in Fig. 2.

Similarly, to determine the regime of the extreme event in the parametric space between f and g, a two-parameter diagram is drawn as shown in Fig. 4. The white regime in the plot shows the extreme events for the combinations of parameter (f, g) separated with the help of Eq. (2) from the nonextreme events (NEE, denoted by the blue color). By comparing Fig. 2(a) with Fig. 4 we can say that EEs occur in the SNA region (however, some of the SNA parameter regime may not contain EEs).

To show the generality of the existence of EEs in the SNA regime, we present the regime of EEs for $\gamma = 0.4$ in the Supplemental Material Figs. S3(a) and S3(b) [30]. This result validates the presence of strange nonchaotic extreme events in the selected parameter regime. In the following section, we characterize the observed behavior as strange and nonchaotic in nature. For this purpose, we perform a singular continuous spectrum analysis and distribution of finite-time Lyapunov exponents.
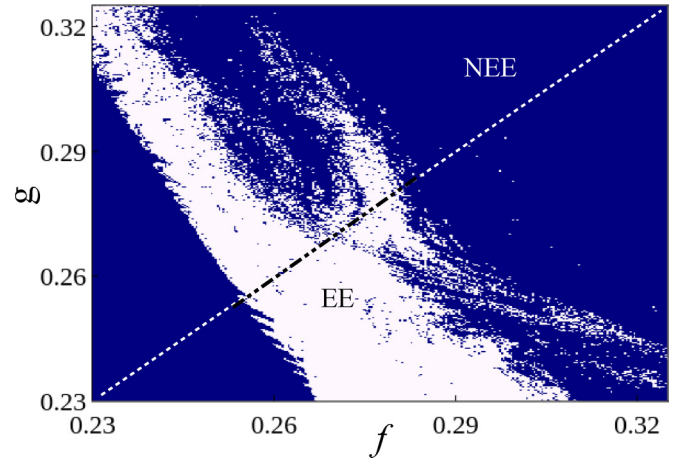
To validate the strange nonchaotic dynamics, we plot a singular continuous spectrum [24,32] in Fig. 5 using a partial Fourier sum of the signal x given by $X(\alpha, N) = \sum_{m=1}^{N} x_m e^{2\pi i m \alpha}$, where α is proportional to the external frequency (ω_1) and N is the length of the time series. The red and black lines show the singular continuous spectrum and the corresponding power-law fit. When N is considered as time, $|X(\alpha, N)|^2$ grows with N, that is, $|X(\alpha, N)|^2 \sim N^\beta$, where β is the slope. When the signal possesses the properties of strange nonchaotic dynamics, the corresponding slope values lie between $1 < \beta < 2$. For this case, the slope value $\beta = 1.576$ confirms the existence of strange nonchaotic dynamics shown in Fig. 5(a). The corresponding path of Brownian motion with a fractal structure in the complex $[\text{Re}(x), \text{Im}(x)]$ plane also confirms the strange nonchaotic dynamics in Fig. 5(b).

The strange nonchaotic dynamics are also validated using another statistical characterization known as the distribution of finite-time Lyapunov exponents. The distribution takes both positive and negative values, but the area under the curve is maximum in the negative regime for strange nonchaotic dynamics. Figure 6 plotted for three different finite-time intervals $T = 500$, 1000, and 1500, where the distribution has a
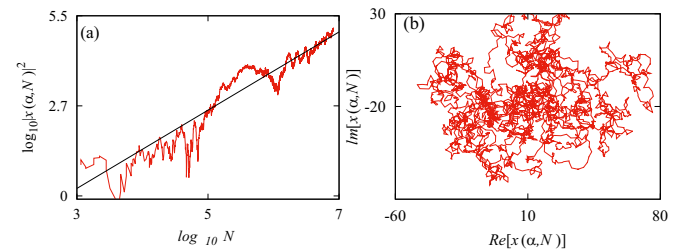

FIG. 5. Singular continuous spectrum for fixing the forcing amplitudes $f, g = 0.278$. (a) The logarithmic plot of $\log_{10} |x(\alpha, N)|^2$ against N. The red and black lines denote the numerical values and the corresponding power-law fit. (b) Fractal path in the complex plane of x. The other parameter values are defined as $\gamma = 0.35$, $\omega_1 = 0.3$, $\omega_2 = (\frac{\sqrt{5}-1}{2})$.
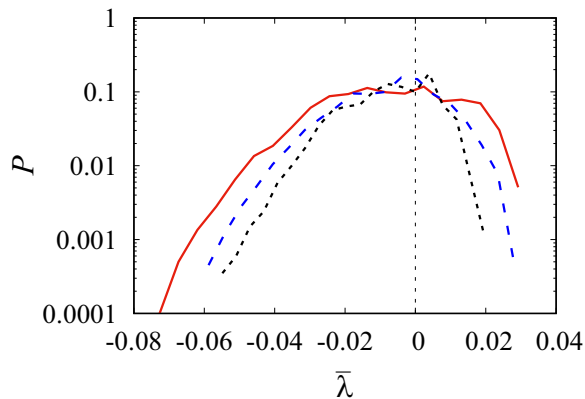
FIG. 6. Finite-time Lyapunov exponent with respect to probability distribution function (PDF) for SNAs by fixing the three distinct finite time periods $T = 500$ (red line), $T = 1000$ (blue dashed line), and $T = 1500$ (black dotted line) with $f, g = 0.278$.

large negative region compared to the positive region showing nonchaotic dynamics. From these analyses, the observed dynamics are strange (nonperiodic) as well as nonchaotic, which also shows the large amplitude and rare events.

The present Letter shows a mechanism of the emergence of extreme events in a quasiperiodically forced Morse oscillator. As a function of forcing amplitude, we found the transition from a quasiperiodic (QP) to chaotic (CH) attractor via strange nonchaotic extreme events. During such extreme event dynamics, we found a long excursion of trajectories that are away from the bounded attractor, while the chaotic attractors show many higher-amplitude peaks. To confirm the existence of EEs, we estimated the critical threshold, and it is observed that the higher-amplitude peaks in the EE cross the critical threshold while the peaks in the CH and QP attractor do not. The dynamical transitions of the attractors and the occurrence of nonchaotic EE dynamics are manifested through maximum Lyapunov exponents. The observed extreme events are further validated using the probability distribution and return interval (interevent interval) with respect to the probability of recurrence times of the EE. Extreme events are abnormal and unexpected events that occur in many natural and man-made systems. Understanding the mechanism or route can help to anticipate the onset of EEs. Early works on extreme events showed the chaotic nature of the extreme events because of the rare and extreme amplitude properties of extreme events. The present study shows an unknown emergence of extreme events that are nonchaotic and nonperiodic extreme events. This finding sheds light on the direction where extreme events can occur as a nonchaotic process.

[1] S. Albeverio, V. Jentsch, and H. Kantz, *Extreme Events in Nature and Society*, The Frontiers Collection (Springer, Berlin, 2006).

[2] R. Höhmann, U. Kuhl, H. J. Stöckmann, L. Kaplan, and E. J. Heller, Phys. Rev. Lett. **104**, 093901 (2010).

[3] J. J. Metzger, R. Fleischmann, and T. Geisel, Phys. Rev. Lett. **112**, 203903 (2014).

[4] A. Mathis, L. Froehly, S. Toenger, F. Dias, G. Genty, and J. M. Dudley, Sci. Rep. **5**, 12822 (2015).

[5] S. Birkholz, C. Brée, I. Veselić, A. Demircan, and G. Steinmeyer, Sci. Rep. **6**, 35207 (2016).

[6] D. Premraj, K. Suresh, S. A. Pawar, L. Kabiraj, A. Prasad, and R. I. Sujith, Europhys. Lett. **134**, 34006 (2021).

[7] A. Saha and U. Feudel, Phys. Rev. E **95**, 062219 (2017).

[8] A. N. Ganshin, V. B. Efimov, G. V. Kolmakov, L. P. Mezhov-Deglin, and P. V. E. McClintock, Phys. Rev. Lett. **101**, 065303 (2008).

[9] H. Bailung, S. K. Sharma, and Y. Nakamura, Phys. Rev. Lett. **107**, 255005 (2011).

[10] D. R. Solli, C. Ropers, P. Koonath, and B. Jalali, Nature (London) **450**, 1054 (2007).

[11] J. Zamora-Munt, B. Garbin, S. Barland, M. Giudici, J. R. Rios Leite, C. Masoller, and J. R. Tredicce, Phys. Rev. A **87**, 035802 (2013).

[12] M. Onorato, T. Waseda, A. Toffoli, L. Cavaleri, O. Gramstad, P. A. E. M. Janssen, T. Kinoshita, J. Monbaliu, N. Mori, A. R. Osborne, M. Serio, C. T. Stansberg, H. Tamura, and K. Trulsen, Phys. Rev. Lett. **102**, 114502 (2009).

[13] S. C. Venkataramani, B. R. Hunt, E. Ott, D. J. Gauthier, and J. C. Bienfang, Phys. Rev. Lett. **77**, 5361 (1996).

[14] C. Grebogi, E. Ott, F. Romeiras, and J. A. Yorke, Phys. Rev. A **36**, 5365 (1987).

[15] J. A. Reinoso, J. Zamora-Munt, and C. Masoller, Phys. Rev. E **87**, 062913 (2013).

[16] S. N. Chowdhury, A. Ray, S. K. Dana, and D. Ghosh, Phys. Rep. **966**, 1 (2022).

[17] E. Mercier, A. Even, E. Mirisola, D. Wolfersberger, and M. Sciamanna, Phys. Rev. E **91**, 042914 (2015).

[18] S. Kumarasamy and A. N. Pisarchik, Phys. Rev. E **98**, 032203 (2018).

[19] A. N. Pisarchik, R. Jaimes-Reátegui, R. Sevilla-Escoboza, G. Huerta-Cuellar, and M. Taki, Phys. Rev. Lett. **107**, 274101 (2011).

[20] A. N. Pisarchik and A. E. Hramov, *Multistability in Physical and Living Systems: Characterization and Applications* (Springer, Berlin, 2022).

[21] F. T. Arecchi, U. Bortolozzo, A. Montina, and S. Residori, Phys. Rev. Lett. **106**, 153901 (2011).

[22] V. Kishore, M. S. Santhanam, and R. E. Amritkar, Phys. Rev. Lett. **106**, 188701 (2011).

[23] A. Kumar, S. Kulkarni, and M. S. Santhanam, Chaos **30**, 043111 (2020).

[24] U. Feudel, S. P. Kuznetsov, and A. S. Pikovsky, *Strange Nonchaotic Attractors: Dynamics Between Order and Chaos in Quasiperiodically Forced Systems* (World Scientific, Singapore, 2006).

[25] A. Prasad, S. S. Negi, and R. Ramaswamy, Int. J. Bifurcation Chaos **11**, 291 (2001).

[26] D. Premraj, K. Suresh, J. Palanivel, and K. Thamilmaran, Commun. Nonlinear Sci. Numer. Simul. **50**, 103 (2017); D. Premraj, K. Suresh, K. Thamilmaran, and K. Rajagopal, Eur. Phys. J. Spec. Top. **231**, 3143 (2022).

[27] G. C. Lie and J. M. Yuan, J. Chem. Phys. **84**, 5486 (1986).

[28] W. Knop and W. Lauterborn, J. Chem. Phys. **93**, 3950 (1990).

[29] S. Zdravkovic, A. N. Bugay, and A. Y. Parkhomenko, Nonlinear Dyn. **90**, 2841 (2017).

[30] See Supplemental Material at http://link.aps.org/supplemental/10.1103/PhysRevE.107.L022201 for the details of time series, phase portraits, and frequency spectrum of the quasi-periodic, strange nonchaotic extreme events and chaotic attractors.

[31] C. Bonatto and A. Endler, Phys. Rev. E **96**, 012216 (2017).

[32] A. S. Pikovsky and U. Feudel, J. Phys. A: Math. Gen. **27**, 5209 (1994).